Climate Simulations Based on a Different-Grid Nested and Coupled Model

Dan Li (丹 利)①, Ji Jinjun (季劲钧) and Li Yinpeng (李银鹏)

Institute of Atmospheric Physics, Chinese Academy of Sciences, Beijing 100029

(Received May 16, 2001; revised April 16, 2002)

ABSTRACT

An atmosphere-vegetation interaction model (AVIM) has been coupled with a nine-layer General Circulation Model (GCM) of Institute of Atmospheic Physics / State Key Laboratory of Numerical Modeling for Atmospheric Sciences and Geophysical Fluid Dynamics (IAP / LASG), which is rhomboidally truncated at zonal wave number 15, to simulate global climatic mean states. AVIM is a model having inter-feedback between land surface processes and eco-physiological processes on land. As the first step to couple land with atmosphere completely, the physiological processes are fixed and only the physical part (generally named the SVAT (soil-vegetation-atmosphere-transfer scheme) model) of AVIM is nested into IAP / LASG L9R15 GCM. The ocean part of GCM is prescribed and its monthly sea surface temperature (SST) is the climatic mean value. With respect to the low resolution of GCM, i.e., each grid cell having longitude 7.5° and latitude 4.5°, the vegetation is given a high resolution of 1.5° by 1.5° to nest and couple the fine grid cells of land with the coarse grid cells of atmosphere. The coupling model has been integrated for 15 years and its last ten-year mean of outputs was chosen for analysis.

Compared with observed data and NCEP reanalysis, the coupled model simulates the main characteristics of global atmospheric circulation and the fields of temperature and moisture. In particular, the simulated precipitation and surface air temperature have sound results. The work creates a solid base on coupling climate models with the biosphere.

Key words: Land surface process (LSP), General circulation model (GCM), Nesting and coupling, Climate simulation

1. Introduction

Since the two important models, BATS (Dickinson et al. 1986) and SiB (Sellers et al. 1986), have been advanced in the 1980s, the simulation of land surface processes (LSP) has improved continuously and many models have been built with various complexities. The SiB model was simplified and developed to be SSiB model (Xue et al. 1991) which decreases the calculated quantities greatly. A model, which focuses on water and heat exchange on land and can be coupled with GCM, was presented by Sun and Lu (1990). Meanwhile, a simple land surface process model for use in climate studies (Ji and Hu 1989) was also advanced and developed later into AVIM (Ji 1995) through incorporating detailed depictions of plant physiological processes. These land models were coupled with atmospheric models to some extent. However, their achievements are at most couplings between physical processes on land and

①E-mail: danli@tea.ac.cn

those in the atmosphere. The physiological and ecological processes of LSP are rarely studied for bidirectional interactions between biosphere and atmosphere due to their complexities. Without biospheric feedback to atmosphere, there is only the one-sided response of biosphere to air. Consequently, an important and promising task for LSP research is to fulfil the complete coupling between biosphere and atmosphere.

2. Simple introduction of models and coupling

AVIM is a land surface process model including both physical transports among soil-vegetation-air and dynamic processes of physiology and ecology (Ji 1995). Unlike other LSP models, its main feature is the dynamic computation of physiological and ecological processes, thus providing a foundation base for the later full coupling of land with air. The model has been tested in different regions with various vegetation types (Ji 1995; Ji and Hu 1999; Ji and Yu 1999), revealing that AVIM has the capacity for simulating physical and biological processes on local and continental scales over surfaces covered by different types of vegetation. In this paper, a snow cover model (Yan and Ji 1995) is incorporated to consider more comprehensive information about the land surface. By analyzing the simulated climatic mean status, it follows that nesting and coupling the fine-grid-cell LSP model with the coarse-grid-cell GCM can improve the climate simulation.

IAP / LASG L9R15 GCM originates from the version of Simmonds (1985), with spherical coordinates in the horizontal direction and σ-coordinate in the vertical. Since the end of 1991, a series of works have been done towards its reformation and development (Wu et al. 1996). A standard stratification of temperature was introduced into the dynamical framework

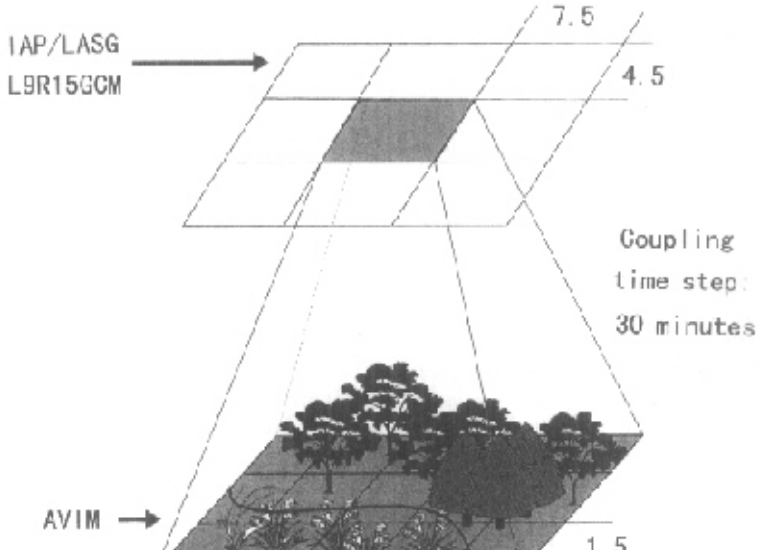

Fig. 1. Skeleton of coupled model.

and the scheme of reduction of a standard atmosphere, an idea, proposed by Zeng (1963) and Phillips (1973), was used to improve model performance. A new k–distribution radiation scheme (Shi 1981; Wang 1996) was implemented into the model to treat cloud processes more reasonably. The model's convection and condensation were parameterized by using the dry–moist convective adjustment scheme (Manabe et al. 1965).

This paper is the first step toward the full coupling of biological processes with the climate model. The physiological part is "frozen", i.e. the leaf area index (LAI) and vegetation cover fraction are prescribed to couple the physical part of AVIM with GCM first. The coupling is bidirectional and simultaneous. The observed global monthly mean of sea surface temperature (SST) from 1979 to 1988 is offered by the international Atmospheric Model Inter–comparison Program (AMIP). The coupling model, with one– layer vegetation and three–layer soil, has nine layers in the vertical atmosphere and is a spectral model rhomboidally truncated at zonal wave number 15 in the horizontal. The resolution of the atmosphere and sea is 7.5° by 4.5°, while the resolution of land is 1.5° by 1.5°. The coupling time step is 30 minutes.

3. Nesting between air and land

The vertical diffusion parts in the prognostic equations of GCM are the main joints between air and land. They depict the exchange of heat, momentum and water vapor between atmosphere and land. Their formulations are expressed as follows:

$$(F_{\rm V}, F_{\rm V}^{T}, F_{\rm V}^{M}) = \frac{g}{P_{*}}\frac{\hat{c}}{\hat{c}\sigma}(\tau, H/c_p, E_{\rm L}) ,$$

$$\tau = \rho C_{\rm D}|V_{\rm a}|V_{\rm a} ,$$

$$H = \rho\delta c_p(\theta_{\rm ac} - \theta_{\rm a})/r_{\rm a} ,$$

$$E_{\rm L} = L\rho(q_{\rm ac} - q_{\rm a})/r_{\rm a} ,$$

$$\delta = (p/p_0)^{R/c_p} .$$

Subscript "v" denotes the vertical direction, thus $F_{\rm V}$, $F_{\rm V}^{T}$, $F_{\rm V}^{M}$ are vertical momentum, heat and water vapor fluxes respectively. $V_{\rm a}$, $\theta_{\rm a}$, $q_{\rm a}$ are air wind speed, potential temperature and specific humidity at the bottom layer of GCM. $\theta_{\rm ac}$, $q_{\rm ac}$, $r_{\rm a}$ are air potential temperature, specific humidity and aerodynamical resistance in the air of canopy, respectively, which are calculated by AVIM. ρ, c_p, $C_{\rm D}$ are air density, specific heat at constant pressure and drag coefficient, and τ, H, $E_{\rm L}$ are transfers of momentum, heat and water vapor fluxes between air and land. P_{*} is the depth of the lowest layer of atmosphere. R is the gas constant.

4. Simulated output analysis

The coupling model is not steady until it is integrated for 5 years. The last ten–year mean of 15 years of integrated output is to be analyzed. Vegetation type data and soil classification data are taken from Li (1999). Initial vegetation data are also provided by Li (1999). Global

soil color grade data are derived from program of BATS (Wilson and Henderson-Sellers 1985) and are interpolated onto the 1.5° by 1.5° grid. The whole global land surface is divided into 12 kinds of vegetation and 1 kind of perpetual ice cover.

4.1 *Surface air temperature analysis*

The coupling model simulates the global surface air temperature comparatively well. Seen in Fig. 2, the observed air temperature in January has a −45°C center in Siberia, but the AVIM coupled simulation, with −50°C, is 5°C less than the observed data, probably due to the influence of high snow albedo. The 0°C isotherm can extend southward to 30°N in Asia in January, corresponding to the observed data. The fact that isotherms located south of 30°N are denser than those of middle and high latitudinal areas, and isotherms along the East Asian coast are also, reveals the intense winter air temperature difference between sea and land. A simulated −45°C center, whose intensity in AVIM is 5°C less than the observed, lies in Greenland. Simulated air temperatures in South America and Africa have some sporadic

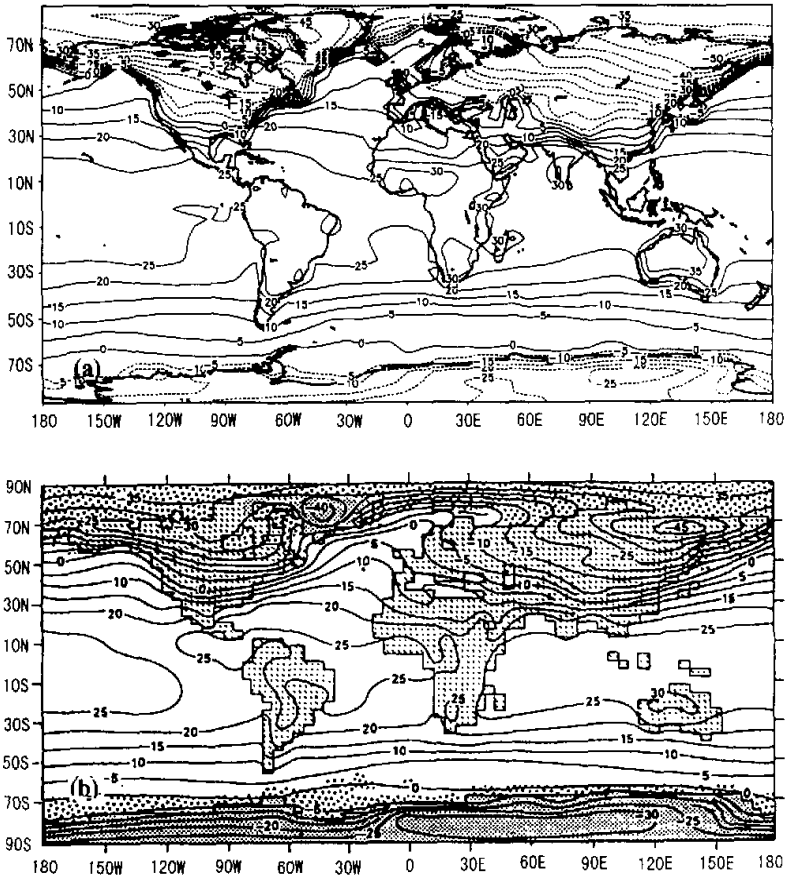

Fig. 2. Monthly mean surface air temperature in January, units: °C. (a) Model output of AVIM+GCM, (b) obseved data from Schlesinger and Gates (1980).

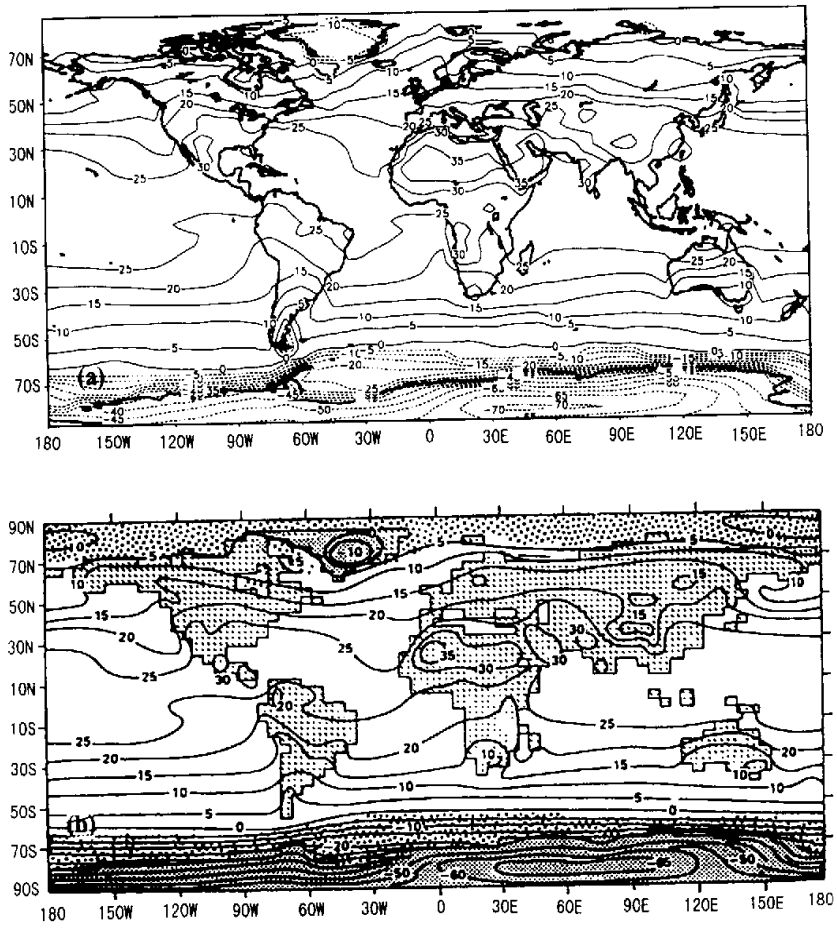

Fig. 3. Monthly mean surface air temperature in July, units °C. (a) Model output of AVIM+GCM, (b) observed data from Schlesinger and Gates (1980)

30°C centers which are 5°C more than the observed data in AVIM. Simulated January air temperature in north of Australia, with its maximal value of 35°C, is 5°C higher than the observed data. The isotherms of the Southern Hemisphere are relatively even and straight, because most areas of that hemisphere are ocean.

Figure 3 shows the simulated and observed monthly mean of July surface air temperature. It follows from the figure that an isotherm of 25°C extends to the south of Asia and a 15°C center is located in the Tibetan Plateau. The air temperature of the Asian continent in July increases intensely and the comparison of the air temperature difference between land and sea is not obvious so that isotherms along East Asian coast are much sparser than those in January. There is a false center of 30°C occupying the estuary of southeast China. The air temperature in high latitudinal areas of Northern Hemisphere in AVIM is close to the observed data. The AVIM coupled model has high temperature areas in America and

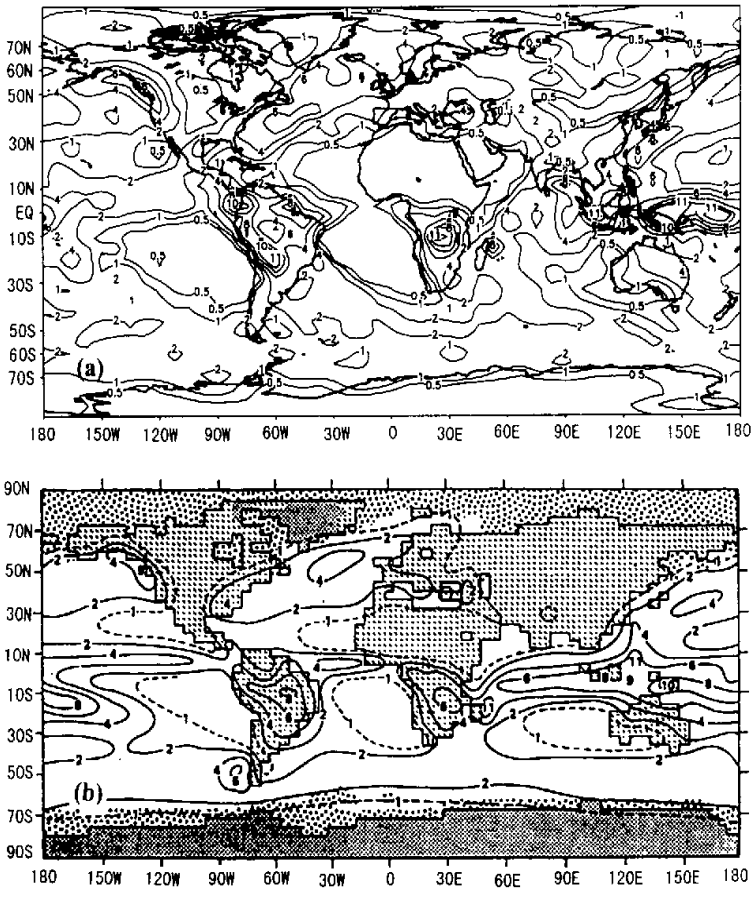

Fig. 4. Monthly mean precipitation in January, units: mm d^{-1}. (a) Model output of AVIM+GCM, (b) model data from Schlesinger and Gates (1980).

northern Africa, and they are also similar to the observed data. The air temperatures of Sahara in July and of Australia in January are higher than the observed, probably demonstrating that the land surface parameters of deserts and arid areas in summer need to be improved.

4.2 Precipitation analysis

Figure 4 presents the simulated and observed January precipitation. It can be seen from the figure that winter precipitation of Asia is scanty, and the precipitation along the East Asian coast approximates reasonably to the observed data. Strong precipitation centers are located at sea, and the heaviest center is located in the west Pacific Ocean "warm pool", which reach 10 mm d^{-1}. However, its range is larger than observed. There are similar areas of 2 mm d^{-1} in Australia, but precipitation in the north of Australia is 2 mm d^{-1} less than the observed. The heavy precipitation, with maximum of 8 mm d^{-1}, of tropical rainforest in

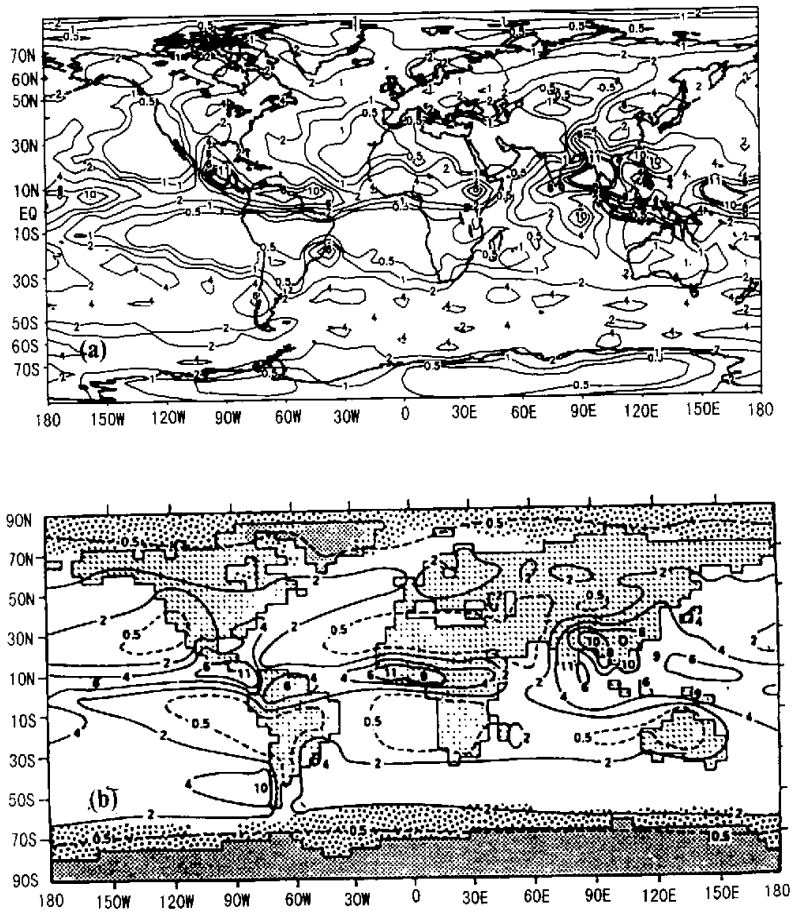

Fig. 5. Monthly mean precipitation in July, units: mm d^{-1}. (a) Model output of AVIM+GCM, (b) observed data from Schlesinger and Gates (1980).

Africa is simulated relatively well, but it is 2 mm d^{-1} more than observed data. The position and range of the precipitation areas of AVIM in Africa are close to the observed data. A small precipitation center stands at the west coast of North America and its simulated intensity is also close to observed data in AVIM, with its simulated range vaster than the observed.

The monthly mean precipitation in July is presented in Fig. 5. Precipitation in Asian monsoon regions is remarkably heavier than that of January. There is a 10 mm d^{-1} precipitation center in the area of Bengal, and the AVIM simulation, with its intensity exceeding 10 mm d^{-1}, is heavier than the observed. Both the observed and the simulated precipitation belts in Southeast Asia show a decreasing trend from southwest to northeast. It is true that the precipitation of middle and high latitudes in Asia is relatively little in July. But unlike the observed data, some small areas of 2 mm d^{-1} are simulated in the region. Compared with the observed data, precipitation is identically below 2 mm d^{-1} in the Australian winter. Simulated

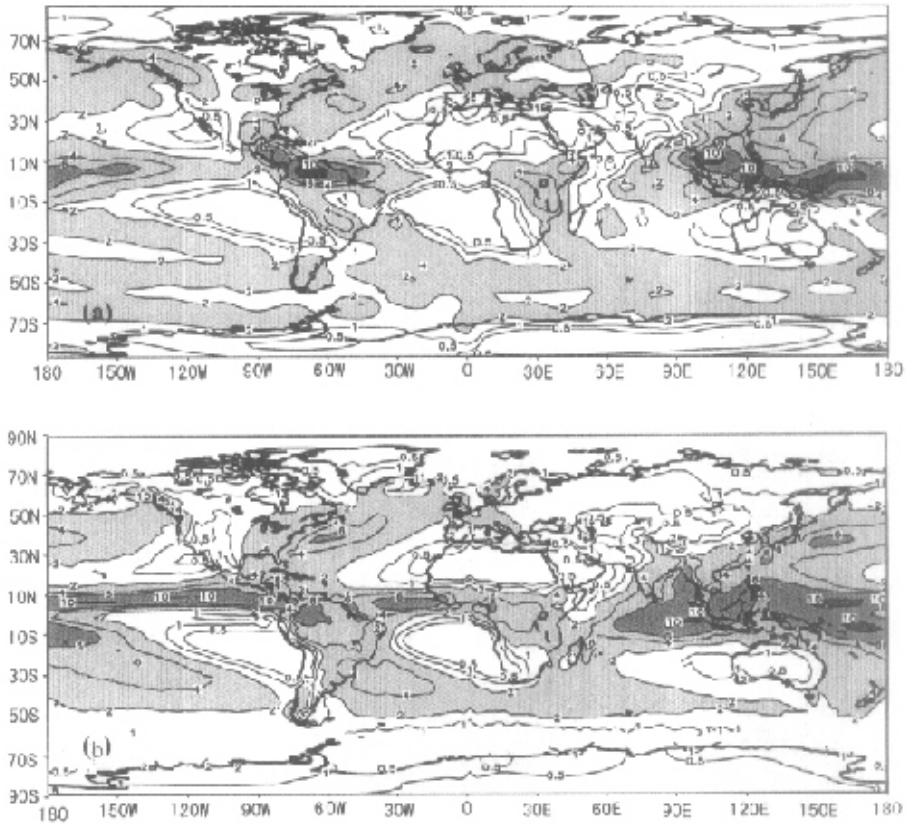

Fig. 6. Annual mean precipitation, units: mm d^{-1}. (a) Model outup of AVIM+GCM, (b) observed data from Xie and Arkin (1997).

precipitation in the center of the African tropical rainforest is less than observed data, whose maximum is 11 mm d^{-1}, and the simulated range is smaller than the observed. American precipitation, mainly located in Latin America and the tropical rainforests of South America, is similar to the observed, with a maximum of 11 mm d^{-1}.

The annual mean of precipitation is presented in Fig. 6 and the simulated data correspond relatively well to the observed. The heaviest precipitation center is located in the Western Pacific with an intensity of 10 mm d^{-1}. The precipitation belt in Southeast Asia shows a decreasing tendency from southwest to northeast. Precipitation in high latitudinal areas is below 1.5 mm d^{-1}. The fact that the precipitation of northeast Australia is more than that of the southwest reveals that the northeast is wetter than the southwest. The simulated center of 4 mm d^{-1} in Africa is more eastward than the observed. The intensity of the precipitation center along the North American west coast is less than the observed data, but its covered range is

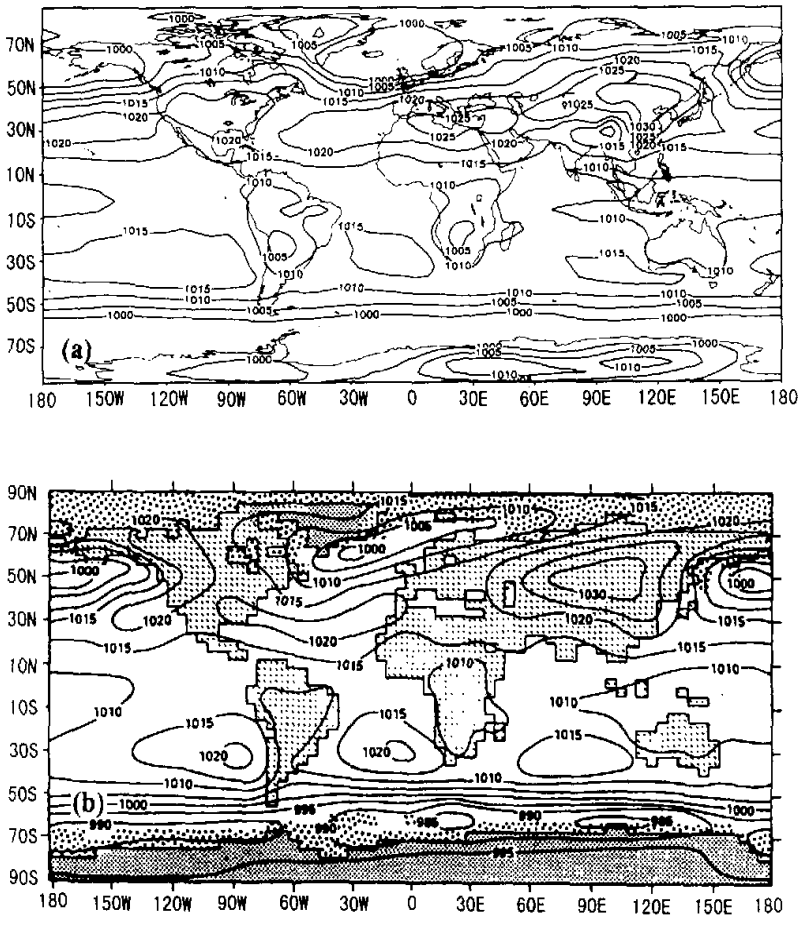

Fig. 7. Monthly mean sea level pressure in January, units: hPa. (a) Model output of AVIM+GCM, (b) observed data from Schlesinger and Gates (1980).

simulated well. The tropical rainforests in South America are so wet that their precipitation can reach 6 mm d^{-1}; however the simulated maximum is 10 mm d^{-1}. The simulated precipitation intensities in the North Atlantic and Pacific are close to the observed.

4.3 *Sea level pressure analysis*

The monthly means of sea level pressure in January and July are presented in Fig. 7 and Fig. 8. It can be seen from the Fig. 7 that several global atmospheric active centers are simulated comparatively well. In January, the strong Siberian cold high which is as high as 1030 hPa occupies the Asian continent, but an unreal low pressure center emerges in the south of the Tibetan Plateau due to the mis-calibration of topography. The simulated intensity of a low pressure center in the south part of Africa is 1005 hPa, which is 5 hPa less than the observed. Australia is encompassed by an isoline of 1010 hPa both in the simulated and ob-

served data. The simulated range of the North American cold high, with a 1020 hPa maximum, is more southward than observed. Yet similarly to the observed, most parts of South America are covered by a 1010 hPa isoline. The Aleutian low, with a 1000 hPa minimum, extends more eastward to the coast of Alaska than observed data. The simulated range of a low-pressure center near Iceland corresponds relatively well to observed data, even though the intensity is 5 hPa less. Three high-pressure centers in the Southern Hemisphere are simulated as corresponding to the observed, but the high-pressure centers in the south Atlantic and south Pacific are 5 hPa less than observed data, which are at 1020 hPa.

In July (Fig. 8), the Asian continent is covered identically by a hot low-pressure center which is as low as 1000 hPa and its position is a little more eastward than the observed data owing to the calibration of topography. The pressure of high latitudes in Asia is 1015 hPa; 5 hPa more than observed. Like the observed, a 1020 hPa high-pressure center emerges in

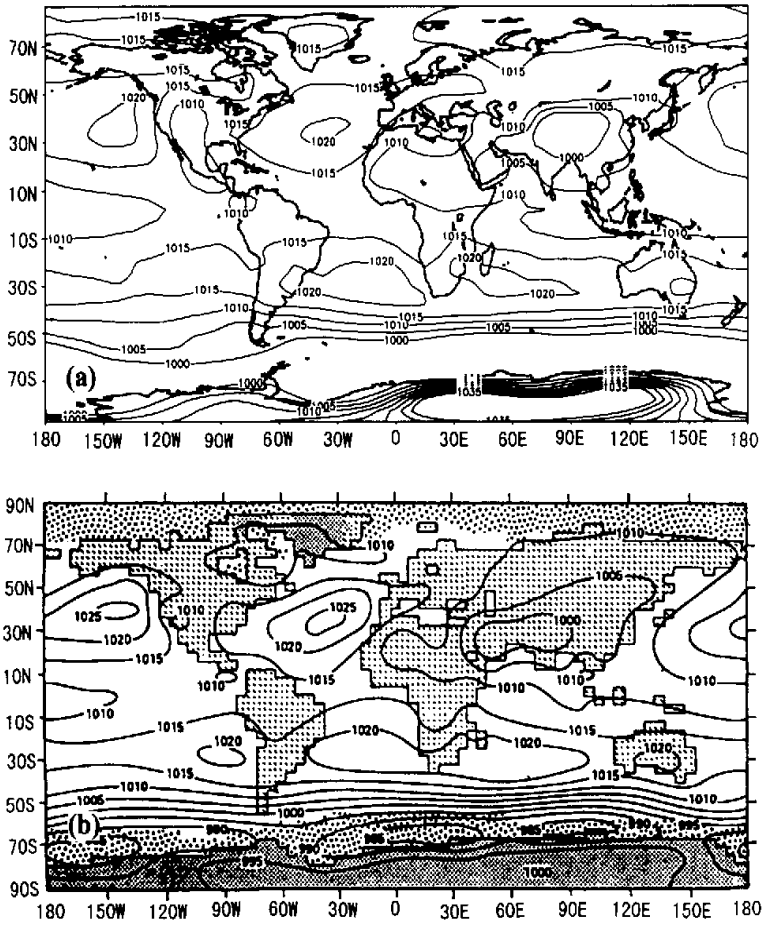

Fig. 8. Monthly mean sea level pressure in July, units: hPa. (a) Model output of AVIM+GCM, (b) observed data from Schlesinger and Gates (1980).

southern Australia. North America is covered by a hot low-pressure center, which is as low as 1010 hPa, with a simulated range larger than observed. The range and axis of direction of the subtropical high at sea in the Northern Hemisphere are simulated comparatively well even though the intensity is 1020 hPa, which is 5 hPa less than observed. The high-pressure center at sea lying to the east of South America is obtained, although it is divided into two centers by the southern end of the continent.

4.4 *Analysis of geopotential height at 500 hPa*

The monthly zonal mean of geopotential height is presented in Fig. 9. The simulations are compared with NCEP reanalysis for lack of observed data and correspond relatively well. The result of the coupled model has an identical tendency as NCEP reanalysis and has no systematic deviation. In January, the simulated results are less than the reanalysis, except for the high latitude of the Southern Hemisphere. The trend of July also corresponds to the NCEP reanalysis while the simulated values are smaller than reanalysis, which reveals that the simulated temperature in the low layer of troposphere is a little less than the observed.

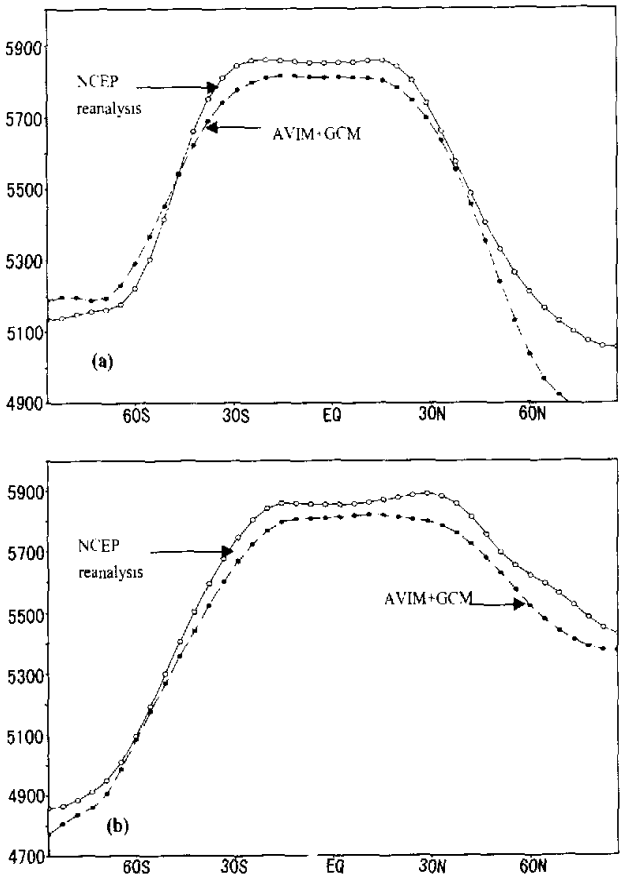

Fig. 9. Monthly zonal mean geoptential height at 500 hPa, units: 10 gpm. (a) Model output of AVIM+GCM and NCEP reanalysis in January, (b) model output of AVIM+GCM and NCEP reanalysis in July.

5. Summary and review

This study is the first step toward full coupling AVIM with GCM by "freezing" the biological and physiological processes in AVIM, (that is, by prescribing leaf area index (LAI) and the vegetation cover fraction), and has coupled the physical part of AVIM with the nine-layer GCM of IAP / LASG. Through the analysis of various output variables of the coupling model, the following conclusions are made:

(1) AVIM delineates the main physical processes on land comparatively well. The coupling model, nesting high a resolution LSP model into GCM, can simulate surface air temperature comparatively well, and the position and intensity of each high or low temperature center correspond reasonably well to the observed data. Coupling AVIM into GCM also improves the global precipitation results. Compared with the 20-year mean of observed data from Xie and Arkin (1997), the simulated annual mean of precipitation is reasonable. But because of the low resolution of GCM, the intense precipitation belt near the equator is simulated poorly.

In addition to these results, other variables, such as sea level pressure in January and July, are simulated comparativly well, and position and intensity of each atmospheric active center correspond in a similar way to the observed. However, the simulated pressure in the south of the Tibetan Plateau is not really low in January due to the calibration of topography. The simulation of sea level pressure along the coast of high latitudes of Asia in July is 5 hPa higher than the observed data, resulting from sporadic snow cover that lowers the air temperature in this region.

(2) After completion of the coupling, further work needs to be done in "unlocking" the biological parts of AVIM and couple the model completely and simultaneously with GCM, classifying the vegetation types on land further and more reasonably.

This paper is financially supported by the NKBRSF (National Key Basic Research Special Funds) project of China (G1999043400), the Key Project of Knowledge Innovation Engineering of Chinese Academy of Sciences (ZKCX2-SW-210), and the Lead Project of Innovation Foundation of Institute of Atmospheric Physics.

REFERENCES

Dan Li, 2000: Simulation of climate based on coupling the atmosphere-vegetation-interaction model (AVIM) with GCM, M.S. thesis, Institute of Atmospheric Physics, Chinese Academy of Sciences, 116pp (in Chinese).

Dickinson, R. E., A. Henderson-Sellers, P. J. Kennedy, and M. F. Wilson, 1986: Biosphere-Atmosphere Transfer Scheme (BATS) for the NCAR Community Climate Model, NCAR / TN-275+STR.

Ji Jinjun, 1995: A climate-vegetation interaction model: Simulating physical and biological processes at the surface. *Journal of Biogeography*, **22**, 445-451.

Ji Jinjun, and Hu Yuchun, 1989: A simple land surface process model for use in climate studies. *Acta Meteorologic Sinica*, **3**, 342-351 (in Chinese).

Ji Jinjun, and Hu Yuchun, 1999: A multi-level canopy model including physical transfer and physiological growth processes. *Climatic and Environmental Research*, **4**, 150-164 (in Chinese).

Ji Jinjun, and Yu Li, 1999: A simulation study of coupled feedback mechanism between physical and biogeochemical processes at the surface. *Chinese Journal of Atmospheric Sciences*, **23**, 439-448 (in Chinese).

Li Yinpeng, 1999: Simulation of carbon exchange between the global ecological system and atmosphere, Post-doctoral report, Institute of Atmospheric Physics, Chinese Academy of Sciences 97pp (in Chinese).

Manabe, S., J. Smagorinsky, and R. F. Strickler, 1965: Simulated climatology of a general circulation model with a hydrological cycle. *Mon. Wea. Rev.*, **93**, 769-798.

Phillips, N. A., 1973: Principles of large scale numerical weather prediction. *Dynamic Meteorology*, P. Morel Ed., Dordrecht-Holland, D. Reidel Publishing Comp., 1-96.

Schlesinger, M. E., and W. Gates, 1980: The January and July performance of the OSU two-level atmospheric general circulation model. *J. Atmos. Sci.*, **37**, 1914-1943.

Sellers, P. J., Y. Mintz, Y. C. Sud, and A. Dalcher, 1986: A simple biosphere model (SiB) for use within general circulation models. *J. Atmos. Sci.*, **43**, 505-531.

Shi G. Y., 1981: An accurate calculation and representation of the infrared transmission function of the atmospheric constituents, Ph. D. Dissertation, Dept. of Sci., Tohoku University of Japan, 191pp.

Simmonds, I., 1985: Analysis of the "spinning" of a global circulation model. *J. Geophys. Res.*, **90**, 5637-5660.

Sun Shufen, and Lu Zhibo, 1990: A ground hydrologic model with inclusion of a layer of vegetation canopy that can interact with general circulation models. *Science in China, Series B*, **33**, 334-344.

Wang Biao, 1996: A radiation transfer model in climate simulations. Ph. D. dissertation, Institute of Atmospheric Physics, Chinese Academy of Sciences, 92pp (in Chinese).

Wilson M. F., and A. Henderson-Sellers, 1985: A global archive of land cover and soils data for use in general circulation climate models. *Journal of Climatology*, **5**, 119-143.

Wu Guoxiong, Liu Hui, Zhao Yucheng, and Li Weiping, 1996: A nine-layer atmospheric general circulation model and its performance. *Advances in Atmosphere Sciences*, **13**, 1-18.

Xie Pingping, and P. A. Arkin, 1997: Global precipitation: A 17-year monthly analysis based on gauge observations, satellite estimates, and numerical model outputs. *Bulletin of the American Meteorological Society*, **78**, 2539-2558.

Xue, Y., P. J. Sellers, J. L. Kinter, and J. Shukla, 1991: A simplified biosphere model for global climate studies. *Journal of Climate*, **4**, 345-364.

Yan Zhongwei, and Ji Jinjun, 1995: Preliminary experiments of a land-surface process model with simple parameterization of snow cover. *Plateau Meteorology*, **14**, 415-424 (in Chinese).

Zeng Qingcun, 1963: Characteristic parameters and dynamical equations of atmospheric motions. *Acta Meteor. Sinica*, **33**, 472-483 (in Chinese).

基于一个不同网格相互嵌套的陆气耦合模式的气候模拟研究

丹 利　季劲钧　李银鹏

摘　要

将一个大气植被相互作用模式(AVIM)与大气所 LASG 的 R15 九层大气环流模式 GOALS 相耦合，用来模拟多年平均的全球气候状况。AVIM 是一个陆地表面陆面和生理过程相互反馈的模型。作为陆气耦合的第一步，暂不考虑 AVIM 中的生理过程，而首先将其物理过程[相当于通常的 SVAT(土壤—植被—大气—传输方案)模型]与大气所 LASG 的九层大气环流模式耦合起来，其中海洋模式部分不参与积分，海面温度是多年平均的气候值。考虑到 GCM 的分辨率较低($7.5^\circ \times 4.5^\circ$)而植被分布必须有较高的分辨率($1.5^\circ \times 1.5^\circ$)，采取了大气与地表面粗细网格的嵌套耦合。模式积分 15 年，取最后 10 年的平均值作分析。将模拟的气候要素场与观测值和 NCEP 再分析资料作了比较，气候模拟结果反映了全球环流与温湿场的主要特征，特别是降水和地面气温的模拟效果较好。这为今后气候模式与生物圈的耦合奠定了一个良好的基础。

关键词：陆面过程，大气环流模式，嵌套耦合，气候模拟